

# Comparing the Performance of Supported Ru Nanocatalysts Prepared by Chemical Reduction of RuCl<sub>3</sub> and Thermal Decomposition of Ru<sub>3</sub>(CO)<sub>12</sub> in the Sunlight-Powered Sabatier Reaction

**Citation for published version (APA):**

Burova, D., Rohlfs, J., Sastre, F., Molina, P. M., Meulendijks, N., Verheijen, M., Kelchtermans, A-S., Elen, K., Hardy, A., Van Bael, M. K., & Buskens, P. J. P. (2022). Comparing the Performance of Supported Ru Nanocatalysts Prepared by Chemical Reduction of RuCl<sub>3</sub> and Thermal Decomposition of Ru<sub>3</sub>(CO)<sub>12</sub> in the Sunlight-Powered Sabatier Reaction. *Catalysts*, 12(3), Article 284. <https://doi.org/10.3390/catal12030284>

**Document license:**  
CC BY

**DOI:**  
[10.3390/catal12030284](https://doi.org/10.3390/catal12030284)

**Document status and date:**  
Published: 02/03/2022

**Document Version:**  
Publisher's PDF, also known as Version of Record (includes final page, issue and volume numbers)

**Please check the document version of this publication:**

- A submitted manuscript is the version of the article upon submission and before peer-review. There can be important differences between the submitted version and the official published version of record. People interested in the research are advised to contact the author for the final version of the publication, or visit the DOI to the publisher's website.
- The final author version and the galley proof are versions of the publication after peer review.
- The final published version features the final layout of the paper including the volume, issue and page numbers.

[Link to publication](#)

**General rights**

Copyright and moral rights for the publications made accessible in the public portal are retained by the authors and/or other copyright owners and it is a condition of accessing publications that users recognise and abide by the legal requirements associated with these rights.

- Users may download and print one copy of any publication from the public portal for the purpose of private study or research.
- You may not further distribute the material or use it for any profit-making activity or commercial gain
- You may freely distribute the URL identifying the publication in the public portal.

If the publication is distributed under the terms of Article 25fa of the Dutch Copyright Act, indicated by the "Taverne" license above, please follow below link for the End User Agreement:

[www.tue.nl/taverne](http://www.tue.nl/taverne)

**Take down policy**







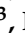
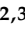
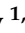


If you believe that this document breaches copyright please contact us at:

[openaccess@tue.nl](mailto:openaccess@tue.nl)

providing details and we will investigate your claim.

## Article

# Comparing the Performance of Supported Ru Nanocatalysts Prepared by Chemical Reduction of RuCl<sub>3</sub> and Thermal Decomposition of Ru<sub>3</sub>(CO)<sub>12</sub> in the Sunlight-Powered Sabatier Reaction

Daria Burova <sup>1,2,3</sup> , Jelle Rohlfs <sup>4</sup> , Francesc Sastre <sup>4</sup> , Pau Martínez Molina <sup>4</sup> , Nicole Meulendijks <sup>4</sup> , Marcel A. Verheijen <sup>5,6</sup> , An-Sofie Kelchtermans <sup>1,2,3</sup> , Ken Elen <sup>1,2,3</sup> , An Hardy <sup>1,2,3</sup> , Marlies K. Van Bael <sup>1,2,3,\*</sup> , and Pascal Buskens <sup>1,4,\*</sup> 

- <sup>1</sup> Institute for Materials Research, Design and Synthesis of Inorganic Materials (DESINE), Hasselt University, Agoralaan Building D, B-3590 Diepenbeek, Belgium; daria.burova@uhasselt.be (D.B.); ansophie.kelchtermans@uhasselt.be (A.-S.K.); ken.elen@uhasselt.be (K.E.); an.hardy@uhasselt.be (A.H.)
- <sup>2</sup> IMEC VZW, IMOMEC Associated Laboratory, Wetenschapspark 1, B-3590 Diepenbeek, Belgium
- <sup>3</sup> EnergyVille, Thor Park 8320, B-3600 Genk, Belgium
- <sup>4</sup> The Netherlands Organisation for Applied Scientific Research (TNO), High Tech Campus 25, 5656AE Eindhoven, The Netherlands; jelle.rohlfstno.nl (J.R.); francesc.sastrecalabuig@tno.nl (F.S.); martinezmolina.pau@gmail.com (P.M.M.); nicole.meulendijks@tno.nl (N.M.)
- <sup>5</sup> Department of Applied Physics, Eindhoven University of Technology, 5600MB Eindhoven, The Netherlands; marcelverheijen@eurofinseag.com
- <sup>6</sup> Eurofins Materials Science, High Tech Campus 11, 5656AE Eindhoven, The Netherlands
- \* Correspondence: marlies.vanbael@uhasselt.be (M.K.V.B.); pascal.buskens@tno.nl (P.B.)



**Citation:** Burova, D.; Rohlfs, J.; Sastre, F.; Molina, P.M.; Meulendijks, N.; Verheijen, M.A.; Kelchtermans, A.-S.; Elen, K.; Hardy, A.; Van Bael, M.K.; et al. Comparing the Performance of Supported Ru Nanocatalysts Prepared by Chemical Reduction of RuCl<sub>3</sub> and Thermal Decomposition of Ru<sub>3</sub>(CO)<sub>12</sub> in the Sunlight-Powered Sabatier Reaction. *Catalysts* **2022**, *12*, 284. <https://doi.org/10.3390/catal12030284>

Academic Editors: Son Ich Ngo and Enrique García-Bordejé

Received: 30 January 2022

Accepted: 1 March 2022

Published: 2 March 2022

**Publisher's Note:** MDPI stays neutral with regard to jurisdictional claims in published maps and institutional affiliations.



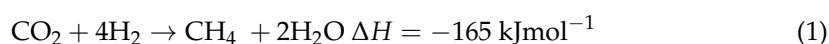
**Copyright:** © 2022 by the authors. Licensee MDPI, Basel, Switzerland. This article is an open access article distributed under the terms and conditions of the Creative Commons Attribution (CC BY) license (<https://creativecommons.org/licenses/by/4.0/>).

**Abstract:** The preparation of Ru nanoparticles supported on  $\gamma$ -Al<sub>2</sub>O<sub>3</sub> followed by chemical reduction using RuCl<sub>3</sub> as a precursor is demonstrated, and their properties are compared to Ru nanoparticles supported on  $\gamma$ -Al<sub>2</sub>O<sub>3</sub> prepared by impregnation of  $\gamma$ -Al<sub>2</sub>O<sub>3</sub> with Ru<sub>3</sub>(CO)<sub>12</sub> and subsequent thermal decomposition. The Ru nanoparticles resulting from chemical reduction of RuCl<sub>3</sub> are slightly larger (1.2 vs. 0.8 nm). In addition, Ru nanoparticles were deposited on Stöber SiO<sub>2</sub> using both deposition techniques. These particles were larger than the ones deposited on  $\gamma$ -Al<sub>2</sub>O<sub>3</sub> (2.5 and 3.4 nm for chemical reduction and thermal decomposition, respectively). Taking into account the size differences between the Ru nanoparticles, all catalysts display similar activity (0.14–0.63 mol·g<sub>Ru</sub><sup>-1</sup>·h<sup>-1</sup>) and selectivity ( $\geq 99\%$ ) in the sunlight-powered Sabatier reaction. Ergo, the use of toxic and volatile Ru<sub>3</sub>(CO)<sub>12</sub> can be avoided, since catalysts prepared by chemical reduction of RuCl<sub>3</sub> display similar catalytic performance.

**Keywords:** carbon dioxide; methane; surface plasmon resonance; photocatalysis; photothermal

## 1. Introduction

As a society, we are currently facing two major challenges: reducing CO<sub>2</sub> emissions and the replacement of fossil fuels with green and sustainable energy sources and carriers. The sunlight-powered conversion of CO<sub>2</sub> to chemicals and fuels simultaneously addresses both challenges. CH<sub>4</sub> is an interesting energy carrier because of its high gravimetric storage density and everyday usage as a fuel. The Sabatier process is a well-known chemical reaction for the conversion of CO<sub>2</sub> and (green) H<sub>2</sub> to CH<sub>4</sub> in the presence of a supported metal catalyst (Equation (1)) [1].



The first and most popular catalyst for this reaction is Ni because of its low cost and wide abundance. Ni promotes CH<sub>4</sub> formation with a selectivity close to 100% [2–4]. These

and other supported metal catalysts for the Sabatier reaction, such as Ru and Rh, require thermal activation at temperatures between 300 and 500 °C [5]. Instead of conventional heating, sunlight is an appealing and green alternative in the case of photo(thermal) catalysis. Catalysts comprising metal nanoparticles with a plasmonic resonance in the UV-vis-NIR region are of interest for sunlight-powered reactions [6]. Based on their localized surface plasmon resonance (LSPR), light illumination induces a resonant response of free electrons in metallic nanoparticles [7,8]. This coherent oscillation dephases non-radiatively and generates hot electrons. These can influence reactions in two ways: they can be transferred to an electron-accepting orbital of an adsorbate in close proximity, or thermalize via electron–electron and electron–phonon scattering increasing the catalyst temperature. The LSPR of metallic nanoparticles can easily be tuned by varying the type of metal, size, shape and architecture of the particle, which makes this concept interesting for visible light and sunlight catalysis [9].

Typical catalysts reported for the (sun)light-powered Sabatier reaction are nanoparticles of group VIII metals supported on metal oxides [10,11]. Even though they do not demonstrate a strong LSPR in the visible light—their LSPR is weak and located in the UV region [12]—they display a strong photoabsorption ability [10]. Ru combines high activity with high selectivity towards CH<sub>4</sub> in the sunlight-powered conversion of CO<sub>2</sub> and H<sub>2</sub> [13,14]. Other examples of group VIII metals reported for this reaction are Au, Pd and Rh [15–17]. The most popular support materials are oxides, for example, Al<sub>2</sub>O<sub>3</sub>, SiO<sub>2</sub>, TiO<sub>2</sub> and CeO<sub>2–x</sub> [18–22]. They prevent the sintering of metal nanoparticles during their synthesis and use, and increase the dispersion and stability of the metal nanoparticle catalyst. The importance of the support material for the stability of the catalyst was demonstrated for Pt nanocatalysts on Al<sub>2</sub>O<sub>3</sub>, where weak electrostatic interaction between support and metal particles led to the formation of agglomerates and, as a consequence, to the loss of the catalytic activity [23]. Supported metal catalysts can be practically applied in different shapes, e.g., as powders and pellets [24,25]. Another key point is the influence of the support material on the reaction mechanism: for Rh and Ru supported on Al<sub>2</sub>O<sub>3</sub>, CO<sub>2</sub> adsorbs on the support, dissociates to CO and O, CO hydrogenates to CHO, then it dissociates to CH and O (rate-determining step, RDS), followed by fast hydrogenation of CH to produce CH<sub>4</sub> [26–28]. On the contrary, on oxide supports with oxygen vacancies such as CeO<sub>2–x</sub>, Ce<sup>3+</sup> acts as a Lewis base and initiates the formation of carboxylate CO<sub>2</sub><sup>δ–</sup>, followed by hydrogenation to formate, which dissociates to form methanol, and, finally methanol is hydrogenated to CH<sub>4</sub>, where the dissociation of formate to methanol is the RDS [29].

In addition to illuminated Ru nanoparticles serving as a nanosource of heat and/or electrons, Lee and coworkers proposed an alternative mechanism to explain the light-induced enhancement of the catalytic process, in which the energy gap of the CO<sub>2</sub> adsorbed on the metallic Ru surface plays a role in increasing the conversion rate and not only the light absorption of the metallic nanoparticle itself [30]. Lee and coworkers proposed that when CO<sub>2</sub> is adsorbed on the Ru (111) surface, its electronic structure changes: the energy gap decreases from 8.5 eV (for the free molecule) to 2.4 eV (CO<sub>2</sub> adsorbed on the Ru surface), and it increases the rate of CO<sub>2</sub> dissociation as the first step in the reaction mechanism.

In this manuscript, we focus on Ru nanoparticles supported on dielectric carrier materials, viz.  $\gamma$ -Al<sub>2</sub>O<sub>3</sub> and Stöber SiO<sub>2</sub>, as catalyst. We selected Ru nanoparticles based on their broadband light absorption, which makes them capable of harvesting a large part of the solar energy, their high catalytic activity and their ability to selectively convert CO<sub>2</sub> and H<sub>2</sub> to CH<sub>4</sub> [31]. Since the CH<sub>4</sub> production costs are dominated by the cost price of green H<sub>2</sub>, there is currently no need to scout for low-cost alternatives to Ru [32]. We excluded semiconductive support materials such as TiO<sub>2</sub> and CeO<sub>2–x</sub>, since they can generate electron-hole pairs using the UV part of sunlight and may directly catalyze the solar methanation reaction.

To validate whether collective effects such as plasmon coupling or collective photothermal heating play a role in the sunlight-powered Ru-catalyzed Sabatier reaction, Grote

et al. [33] studied spheroidal Ru-nanoparticles on  $\gamma$ -Al<sub>2</sub>O<sub>3</sub> support, synthesized by impregnation of  $\gamma$ -Al<sub>2</sub>O<sub>3</sub> with Ru<sub>3</sub>(CO)<sub>12</sub> followed by high temperature annealing under N<sub>2</sub>. They observed that the activity of the catalyst upon sunlight illumination increased superlinearly with a higher loading of metal in the catalyst. This effect was attributed to collective photothermal heating, which was further supported by continuous flow experiments [34] and multipoint temperature measurements inside the illuminated catalyst bed [35].

Since Ru<sub>3</sub>(CO)<sub>12</sub> is a volatile chemical which is acutely toxic upon inhalation, we scouted a non-volatile precursor to prepare Ru nanospheres on metal oxide supports. For that purpose, we applied RuCl<sub>3</sub> using a deposition-precipitation sequence, followed by chemical reduction to obtain Ru nanoparticles similar to the ones obtained via thermal decomposition of Ru<sub>3</sub>(CO)<sub>12</sub>. Although the preparation of supported Ru catalysts using a deposition-precipitation sequence has been reported previously [18,36], the performance of catalysts produced in that manner has never been validated in comparison to Ru<sub>3</sub>(CO)<sub>12</sub>-derived catalysts for the sunlight-powered Sabatier reaction. The research question of the study at hand is whether the preparation technique affects the catalyst's chemical composition and nanostructure, and consequently the functional performance of the catalyst in the sunlight-powered Sabatier reaction. To address this question, we compare the catalytic performance of Ru nanoparticles prepared by impregnation and thermal decomposition of Ru<sub>3</sub>(CO)<sub>12</sub> and deposition-precipitation and chemical reduction using RuCl<sub>3</sub> on two different dielectric metal oxide supports, viz. Stöber SiO<sub>2</sub> and  $\gamma$ -Al<sub>2</sub>O<sub>3</sub>. Availability of information on the relationship between the preparation technique, chemical composition and nanostructure, and functional performance facilitates the design and discovery of new nanocatalysts [37].

## 2. Results and Discussion

### 2.1. Synthesis and Characterization of Ru/SiO<sub>2</sub> and Ru/Al<sub>2</sub>O<sub>3</sub> Catalysts

Two different methods were used for decoration of the supports, viz.  $\gamma$ -Al<sub>2</sub>O<sub>3</sub> and Stöber SiO<sub>2</sub>, with Ru nanoparticles: (1) deposition-precipitation followed by chemical reduction using RuCl<sub>3</sub> as a precursor (CR), and (2) impregnation with Ru<sub>3</sub>(CO)<sub>12</sub> and subsequent high-temperature decomposition (TD). An overview of all catalysts prepared in this study is provided in Table 1. The composition and structure of these catalysts and their catalytic performance are compared to previous results obtained with Al<sub>2</sub>O<sub>3</sub>-TD catalysts [33].

**Table 1.** Catalysts prepared with different Ru loading (% *w/w*, obtained by ICP-EOS analyses) using Ru<sub>3</sub>(CO)<sub>12</sub> and subsequent high-temperature decomposition (marked with TD) and deposition-precipitation followed by chemical reduction using RuCl<sub>3</sub> as a precursor (marked with CR).

Carrier Material	Loading, %			
SiO <sub>2</sub> -TD	4.84	3.49	2.15	0.96
SiO <sub>2</sub> -CR	3.88	3.34	2.05	0.98
Al <sub>2</sub> O <sub>3</sub> -CR	3.89	-	-	-

#### 2.1.1. Deposition-Precipitation with Following Chemical Reduction (CR) Using RuCl<sub>3</sub>

A slurry and dispersion of  $\gamma$ -Al<sub>2</sub>O<sub>3</sub> and Stöber SiO<sub>2</sub>, respectively, were prepared in aqueous urea. RuCl<sub>3</sub> and HCl were added to the mixture and then treated at 80 °C for 5 h to perform the deposition of Ru<sup>3+</sup> and precipitation of ruthenium(III) oxide-hydroxide species on the surface of the support. Then, NaBH<sub>4</sub> was added to reduce the deposited ruthenium(III) oxide-hydroxide and form Ru nanoparticles. For Stöber SiO<sub>2</sub> as support, four different quantities of RuCl<sub>3</sub> were added to produce catalyst powders with theoretical Ru loadings of 1, 2.5, 4 and 6% *w/w*. For  $\gamma$ -Al<sub>2</sub>O<sub>3</sub> as support, we aimed at preparing one catalyst with a theoretical Ru loading of 6% *w/w*. The resulting black catalyst materials were characterized using inductively coupled plasma optical emission spectrometry (ICP-OES, Table 1) to determine the Ru content and transmission electron microscopy (TEM,

Figure 1) to determine the size and shape of the Ru nanoparticles and their distribution over the  $\text{SiO}_2$  and  $\text{Al}_2\text{O}_3$  support surfaces.

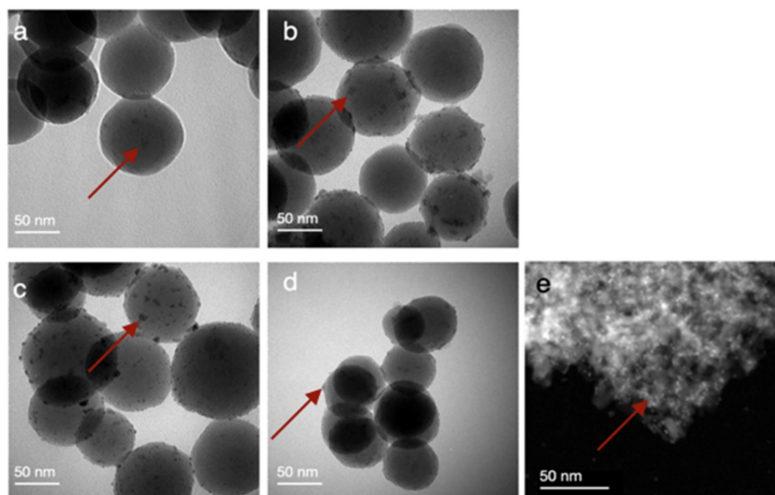


**Figure 1.** Bright-field TEM images of Ru nanoparticle catalysts on  $\text{SiO}_2$  and  $\gamma\text{-Al}_2\text{O}_3$  prepared by deposition-precipitation with following chemical reduction using  $\text{RuCl}_3$ , and with a Ru loading on silica of (a) 0.98%  $w/w$ , (b) 2.05%  $w/w$ , (c) 3.34%  $w/w$  and (d) 3.88%  $w/w$ , (e) and on alumina of 3.89%  $w/w$  (high-angle annular dark-field scanning transmission electron microscopy). The red arrows illustratively point out a supported Ru nanoparticle.

ICP-OES analyses performed on catalysts digested in a mixture of  $\text{HCl}$ ,  $\text{HNO}_3$  and  $\text{HF}$  yielded practically achieved Ru loadings of 0.98, 2.05, 3.34 and 3.88%  $w/w$  on Stöber  $\text{SiO}_2$  (for 1, 2.5, 4 and 6%  $w/w$  theoretical loading) and 3.89%  $w/w$  (for 6%  $w/w$  theoretical loading) on  $\gamma\text{-Al}_2\text{O}_3$ . The TEM analyses demonstrate that small spheroidal Ru particles are randomly distributed over the surface of the Stöber  $\text{SiO}_2$  (Figure 1a–d) and  $\gamma\text{-Al}_2\text{O}_3$  (Figure 1e). The size of the Ru nanoparticles deposited on Stöber  $\text{SiO}_2$  ( $d = 50 \pm 5$  nm) was  $2.5 \pm 0.8$  nm and remained constant with increasing Ru loading. Some agglomerates were observed, and their size did not exceed 8.9 nm. The size of the Ru nanoparticles deposited on  $\gamma\text{-Al}_2\text{O}_3$  was  $1.2 \pm 0.5$  nm and no agglomerates were observed. This is larger than the size previously reported for Ru nanoparticles on  $\gamma\text{-Al}_2\text{O}_3$  obtained via thermal decomposition (0.8 nm) [33]. In previous work, we have confirmed that Ru nanoparticles obtained via thermal decomposition of  $\text{Ru}_3(\text{CO})_{12}$  are metallic in nature, and excluded the presence of  $\text{RuO}_2$  [33]. To confirm this for the catalysts prepared via chemical reduction of  $\text{RuCl}_3$ , we performed XRD analysis. Due to the low loading and small particle size, however, Ru reflections could not be detected (Figure S1). Furthermore, we performed thermogravimetric analyses (TGA) in air to evaluate if we could detect a mass increase in the sample because of the oxidation of Ru to  $\text{RuO}_2$  at elevated temperatures (Figure S2). A mass decrease of about 10% due to the loss of adsorbed water and progressive condensation of  $\text{Si-OH}$  and  $\text{Al-OH}$  groups made it impossible to detect a potential small increase (<1% expected) due to the oxidation of Ru. Since we observe no increase in the reaction rate over time (see Section 2.2.), which we previously observed when using supported  $\text{RuO}_2$  catalysts that reduced to metallic Ru during the first minutes of the reaction [14], we assume that our catalysts comprise metallic Ru.

### 2.1.2. Impregnation with $\text{Ru}_3(\text{CO})_{12}$ and Subsequent Thermal Decomposition (TD)

For the second method, the procedure reported by Grote et al. [33] was used: the impregnation of Stöber  $\text{SiO}_2$  with  $\text{Ru}_3(\text{CO})_{12}$  as ruthenium precursor followed by high-temperature treatment in an inert atmosphere. The loading of Ru was controlled by the ratio of  $\text{Ru}_3(\text{CO})_{12}$  to support material. ICP-OES analyses showed Ru loadings of 0.96, 2.15, 3.49 and 4.84%  $w/w$  on Stöber  $\text{SiO}_2$ , when aiming for theoretical loadings of 1, 2.5, 4

and 6% *w/w* (Table 1). TEM analyses demonstrated a homogeneous dispersion of small spheroidal ruthenium nanoparticles of larger size than the ones obtained using RuCl<sub>3</sub> for all Ru loadings ( $3.4 \pm 1.2$  vs.  $2.5 \pm 0.8$  nm, Figure 2).

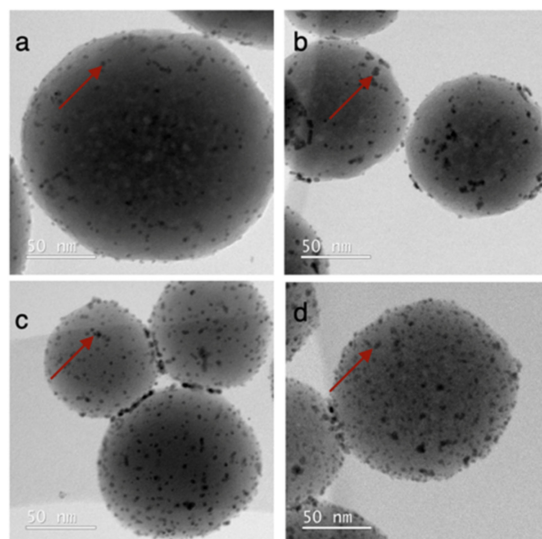


**Figure 2.** TEM analyses of Ru nanoparticle catalysts on SiO<sub>2</sub>, prepared by impregnation with Ru<sub>3</sub>(CO)<sub>12</sub> and subsequent thermal decomposition, and with a Ru loading of (a) 0.96% *w/w*, (b) 2.15% *w/w*, (c) 3.49% *w/w* and (d) 4.84% *w/w*. The red arrows illustratively point out a supported Ru nanoparticle.

## 2.2. Catalyst Performance in the Sunlight-Powered Sabatier Reaction

Our previous work demonstrated that Ru nanoparticles supported on  $\gamma$ -Al<sub>2</sub>O<sub>3</sub>, prepared via impregnation with Ru<sub>3</sub>(CO)<sub>12</sub> and subsequent thermal decomposition, are efficient catalysts for the sunlight-powered Sabatier reaction [33]. To investigate whether the way of production affects the catalytic performance, comparative experiments with Ru/Al<sub>2</sub>O<sub>3</sub> produced via deposition-precipitation followed by chemical reduction using RuCl<sub>3</sub> were carried out (Ru/Al<sub>2</sub>O<sub>3</sub>-CR, 3.89% *w/w*). To determine the activity of the catalyst in the sunlight-powered Sabatier process, Ru/Al<sub>2</sub>O<sub>3</sub>-CR was tested at a catalyst bed temperature of approximately 220 °C, realized via combined heating of the reactor to a starting temperature of 150 °C and illumination. In the latter case, a solar simulator illuminated the catalyst bed with a light intensity of 6.6 suns resulting in a catalyst bed temperature of approximately 220 °C. Under these conditions, CH<sub>4</sub> was produced as the sole reaction product at a starting rate of 0.46 mol·g<sub>Ru</sub><sup>-1</sup>·h<sup>-1</sup> (Figure 3).

This value is slightly lower than the previously reported activity for Ru/Al<sub>2</sub>O<sub>3</sub> produced via impregnation with Ru<sub>3</sub>(CO)<sub>12</sub> and subsequent thermal decomposition (TD, 0.63 mol·g<sub>Ru</sub><sup>-1</sup>·h<sup>-1</sup>, Figure 3). For the dark reaction with both catalysts at 220 °C, we observed a reaction rate of 0.49 mol·g<sub>Ru</sub><sup>-1</sup>·h<sup>-1</sup>(CR) and 0.29 mol·g<sub>Ru</sub><sup>-1</sup>·h<sup>-1</sup> (TD, Figure 3).

Overall, the catalytic activity and selectivity of Ru/Al<sub>2</sub>O<sub>3</sub>-TD and Ru/Al<sub>2</sub>O<sub>3</sub>-CR are within the same order of magnitude. Potential reasons for the observed minor differences in activity between catalysts prepared with different Ru deposition techniques may be the presence of remaining species that block catalytic sites in the catalyst produced via chemical reduction, and the larger particle size of the Ru nanoparticles obtained from RuCl<sub>3</sub> (1.2 vs. 0.8 nm [33]). Based on the catalytic performance of the Ru/Al<sub>2</sub>O<sub>3</sub> catalyst, we conclude that the deposition-precipitation followed by the chemical reduction is a suitable alternative method for producing Ru nanocatalysts. The result of the catalytic experiments demonstrates that the use of volatile and toxic Ru<sub>3</sub>(CO)<sub>12</sub> can be avoided. Besides the preparation method, two carrier materials—Stöber SiO<sub>2</sub> and  $\gamma$ -Al<sub>2</sub>O<sub>3</sub>—were compared under identical reaction conditions using both preparation methods. Samples with similar Ru loading were taken for comparison (between 3.49% *w/w* and 3.89% *w/w*

Ru). The conversion-time profile for Ru/SiO<sub>2</sub> obtained by the deposition-precipitation with chemical reduction almost coincides with that of Ru/Al<sub>2</sub>O<sub>3</sub> obtained by the same method, reflected by their initial reaction rates of 0.37 mol·g<sub>Ru</sub><sup>-1</sup>·h<sup>-1</sup> for Ru/SiO<sub>2</sub>-CR vs. 0.46 mol·g<sub>Ru</sub><sup>-1</sup>·h<sup>-1</sup> for Ru/Al<sub>2</sub>O<sub>3</sub>-CR (Figure 4). In the absence of H<sub>2</sub>, Ru catalysts prepared by chemical reduction of RuCl<sub>3</sub> do not promote conversion of CO<sub>2</sub> to CH<sub>4</sub> or other products. In previous work, we have also demonstrated this for Ru catalysts prepared via thermal decomposition of Ru<sub>3</sub>(CO)<sub>12</sub> [33].

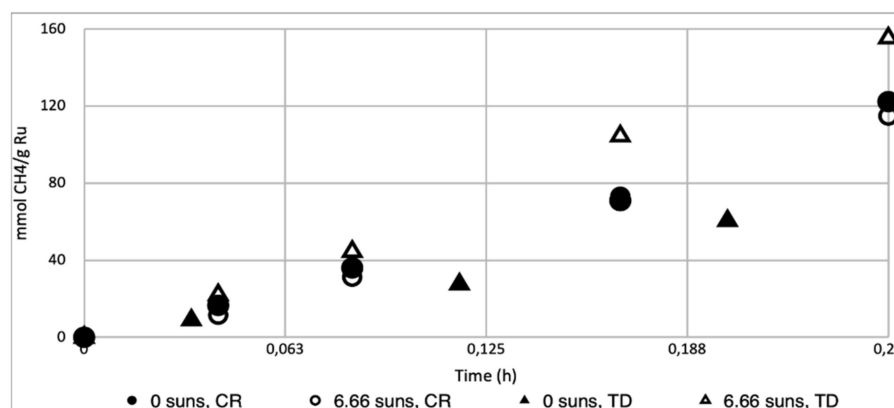


**Figure 3.** Conversion-time profile for the Sabatier reaction carried out in dark (0 suns) and light conditions (6.66 suns) with Ru/Al<sub>2</sub>O<sub>3</sub> catalysts prepared using Ru<sub>3</sub>(CO)<sub>12</sub> (TD, 3.6% w/w Ru) [33] and RuCl<sub>3</sub> (CR, 3.89% w/w). Reaction conditions for all experiments: reaction mixture of H<sub>2</sub>/CO<sub>2</sub>/N<sub>2</sub> (4.5:1:1) at 3.5 ± 0.2 bar pressure, 200 mg of Ru/Al<sub>2</sub>O<sub>3</sub> or Ru/SiO<sub>2</sub> catalyst, catalyst bed temperature of approximately 220 °C.

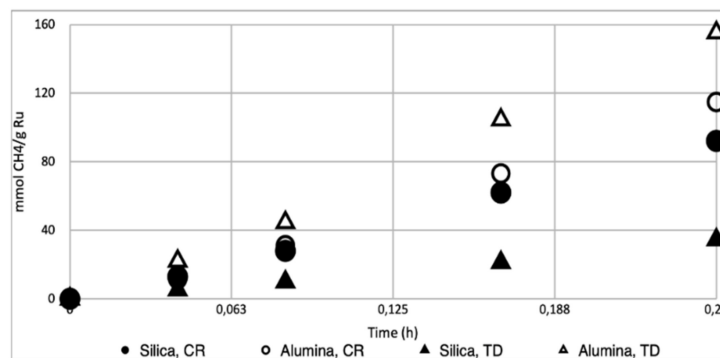


**Figure 4.** Conversion-time profile for the Sabatier reaction carried out in light conditions (6.66 suns) with Ru/Al<sub>2</sub>O<sub>3</sub> catalysts prepared using Ru<sub>3</sub>(CO)<sub>12</sub> (TD, 3.6% w/w Ru, Δ) [33] and RuCl<sub>3</sub> (CR, 3.89% w/w, ○), and their SiO<sub>2</sub> supported counterparts Ru/SiO<sub>2</sub>-TD (3.49% w/w, ▲) and Ru/SiO<sub>2</sub>-CR (3.88% w/w, ●). Reaction conditions for all experiments: reaction mixture of H<sub>2</sub>/CO<sub>2</sub>/N<sub>2</sub> (4.5:1:1) at 3.5 ± 0.2 bar pressure, 200 mg of Ru/Al<sub>2</sub>O<sub>3</sub> or Ru/SiO<sub>2</sub> catalyst, catalyst bed temperature of approximately 220 °C.

However, for the catalysts obtained using thermal decomposition of Ru<sub>3</sub>(CO)<sub>12</sub>, the slope of the Ru/SiO<sub>2</sub>-TD curve showed a lower initial rate than Ru/Al<sub>2</sub>O<sub>3</sub>-TD [33] (0.14 vs. 0.63 mol·g<sub>Ru</sub><sup>-1</sup>·h<sup>-1</sup>). This is caused by the substantial difference in Ru particle size for catalysts and related surface area obtained using both preparation techniques: 3.4 nm for Ru/SiO<sub>2</sub>-TD vs. 0.8 nm for Ru/Al<sub>2</sub>O<sub>3</sub>-TD.

To validate their potential for reuse, we evaluated the catalytic performance of Ru/SiO<sub>2</sub>-TD and Ru/SiO<sub>2</sub>-CR with Ru loadings of 3.49% w/w and 3.34% w/w, respectively, in three sequential reaction runs. In all of these experiments, we combined sunlight illumination (6.66 suns) with conventional heating of the reactor to achieve a catalyst bed temperature

of 220 °C. For the experiments performed with Ru/SiO<sub>2</sub>-TD, we observed a similar reaction rate in all three runs (0.14 mol·g<sub>Ru</sub><sup>-1</sup>·h<sup>-1</sup> in run 1, 0.15 mol·g<sub>Ru</sub><sup>-1</sup>·h<sup>-1</sup> in run 2 and 0.14 mol·g<sub>Ru</sub><sup>-1</sup>·h<sup>-1</sup> in run 3) (Figure S3). For the experiments performed with Ru/SiO<sub>2</sub>-CR, we observed a decrease in reaction rate from run 1 to run 3 of 28% (0.37 mol·g<sub>Ru</sub><sup>-1</sup>·h<sup>-1</sup> in run 1, 0.35 mol·g<sub>Ru</sub><sup>-1</sup>·h<sup>-1</sup> in run 2 and 0.27 mol·g<sub>Ru</sub><sup>-1</sup>·h<sup>-1</sup> in run 3). This may be explained by progressive agglomeration of Ru on the SiO<sub>2</sub> surface during the catalytic reactions, as illustrated by bright-field (BF) TEM analyses of the same catalyst before run 1 and after run 3 (Figure 5). The degree of agglomeration is 52%, and typical agglomerate sizes are 9.5 nm (Figure S4).

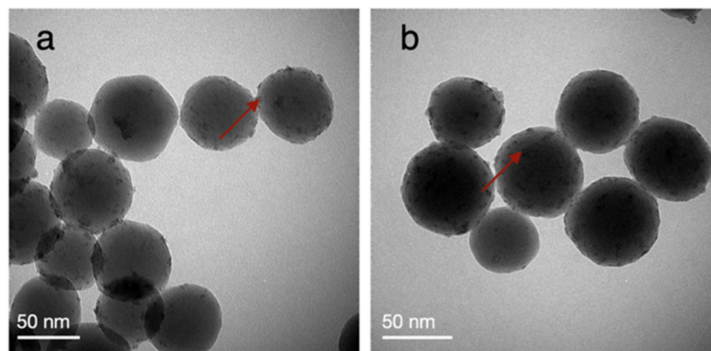


**Figure 5.** BFTEM images of Ru/SiO<sub>2</sub>-CR with a Ru loading of 3.34% *w/w* (a) before and (b) after sunlight-powered Sabatier's reaction. Reaction conditions: reaction mixture of H<sub>2</sub>/CO<sub>2</sub>/N<sub>2</sub> (4.5:1:1) at 3.5 ± 0.2 bar pressure, 200 mg of Ru/Al<sub>2</sub>O<sub>3</sub> or Ru/SiO<sub>2</sub> catalyst, light intensity of 6.66 suns, catalyst bed temperature of approximately 220 °C. The red arrows illustratively point out a supported Ru nanoparticle.

### 3. Materials and Methods

#### 3.1. Catalyst Synthesis

##### 3.1.1. Synthesis of Stöber SiO<sub>2</sub> Support

SiO<sub>2</sub> nanoparticles were prepared according to the Stöber process by hydrolysis and condensation of tetraethyl orthosilicate (TEOS) [38]. For the preparation of 50 nm sized SiO<sub>2</sub> particles, ethanol (40 mL, VWR Chemicals, Radnor, PA, USA, 98%), H<sub>2</sub>O (1 mL, milliQ grade), and aqueous ammonia (3 mL, VWR Chemicals, Radnor, PA, USA, 32% in water) were mixed in a 250 mL flask and stirred for 5 min. Then, TEOS (4 mL) dissolved in EtOH (30 mL) was added. The mixture was stirred at 25 °C for 5 h. The obtained SiO<sub>2</sub> nanoparticles were washed twice with water (milliQ grade) after 10 min centrifugation (11,000 × *g* rpm) and dried at 100 °C for 2 h.

##### 3.1.2. Synthesis of Ru/SiO<sub>2</sub> Catalyst: Deposition-Precipitation with Following Chemical Reduction Using RuCl<sub>3</sub>

For the synthesis of Ru/SiO<sub>2</sub> with a theoretical Ru loading of 2.5 *w/w*%, Stöber SiO<sub>2</sub> nanoparticles (400 mg) were dispersed in an aqueous urea solution (20 mL, 2.5 M in milliQ water, ACROS Organics, Geel, Belgium, 99%), after which an aqueous solution of ruthenium (III) chloride hydrate (0.02 M in 0.1 M HCl; Aldrich, St. Louis, MO, USA, 40–49% ruthenium; HCl, VWR Chemicals, Radnor, PA, USA, 37% in water; 5 mL) was added and ultrasonicated for 10 min. Next, the resulting mixture was heated for 5 h at 80 °C. After that, NaBH<sub>4</sub> solution (0.01 M in milliQ water; 5 mL) was added and the reaction mixture was further heated for 30 min. Finally, the Ru/SiO<sub>2</sub> catalyst particles were filtered and washed three times with water and once with ethanol. The catalyst was dried at room temperature for 24 h and stored in ambient conditions.



### 3.1.3. Synthesis Ru/SiO<sub>2</sub> Catalyst: Impregnation with Ru<sub>3</sub>(CO)<sub>12</sub> and Subsequent Thermal Decomposition

This synthesis was performed in analogy to the protocol reported by Grote et al. for Ru/ $\gamma$ -Al<sub>2</sub>O<sub>3</sub> [33]: Ru<sub>3</sub>(CO)<sub>12</sub> (ACROS Organics, Geel, Belgium, 99%) was dissolved in tetrahydrofuran (THF, VWR Chemicals, Radnor, PA, USA, GPR RECTAPUR grade, 99%) by stirring at room temperature for 30 min. After the silica nanoparticles were added to the solution, the resulting mixture was stirred for 2 h at room temperature, whereafter the THF was removed by rotary evaporation under reduced pressure at 80 °C. The precursor was decomposed under a N<sub>2</sub> inert gas atmosphere with a heating ramp of 5 °C·min<sup>-1</sup> until 300 °C and kept at 300 °C for 2 h, cooled down to room temperature and stored in ambient conditions.

### 3.1.4. Synthesis of Ru/Al<sub>2</sub>O<sub>3</sub> Catalyst: Deposition-Precipitation with Following Chemical Reduction Using RuCl<sub>3</sub>

$\gamma$ -Al<sub>2</sub>O<sub>3</sub> (Alfa Aesar, Haverhill, MA, USA, 99.97%, surface area 200 m<sup>2</sup>·g<sup>-1</sup>) was calcined in air at 500 °C for 6 h. After cooling down to room temperature, the same procedure was carried out as for Ru/SiO<sub>2</sub> (procedure 2).

## 3.2. Characterization of the Catalyst

### 3.2.1. Dynamic Light Scattering

The particle size of Stöber SiO<sub>2</sub> and its distribution were characterized via dynamic light scattering (DLS), using a Brookhaven ZetaPals machine (Brookhaven Instruments Corporation, Holtsville, NY, USA). The Stöber SiO<sub>2</sub> particles were dispersed in milliQ water at pH = 7.5, and then measured in dispersion.

### 3.2.2. Electron Microscopy

The particle size and morphology of Ru/Al<sub>2</sub>O<sub>3</sub> and Ru/SiO<sub>2</sub> catalysts were investigated using an FEI Tecnai Spirit Twin electron microscope (Thermo Fischer Scientific, Hillsboro, OR, USA). Imaging was performed in bright-field transmission electron microscopy (TEM) and high-angle annular dark field (HAADF) scanning transmission electron microscopy (STEM) mode. Samples for (S)TEM investigation were prepared by mixing the catalyst powder with ethanol, followed by deposition of the resulting suspension onto a Cu-supported holey carbon grid. Using the FEI Tecnai Spirit Twin electron microscope equipped with a Si (Li) Ametek EDX detector for energy-dispersive X-ray analysis, the Ru loading was analyzed. The number of Ru particle agglomerates was counted by analysis of all STEM pictures of each sample, listing and then determining the number of agglomerates by counting the particles with the diameter larger than the mean diameter of single Ru nanoparticle on the image. STEM-EDX mappings were acquired using a probe-corrected JEOL ARM 200F (Peabody, MA, USA), equipped with a 100 mm<sup>2</sup> SDD Centurio EDX detector.

### 3.2.3. Inductively Coupled Plasma Optical Emission Spectrometry

The Ru content of the catalysts was determined by inductively coupled plasma optical emission spectrometry (ICP-OES, Perkin Elmer Optima 3300 dv simultaneous spectrometer, PerkinElmer, Waltham, MA, USA). For Ru content analysis, catalyst (20 mg) was added to a teflon vessel with HCl (6 mL, VWR Chemicals, Radnor, PA, USA, 37%), HNO<sub>3</sub> (1 mL, VWR Chemicals, Radnor, PA, USA, 69%) and HF (3 mL, VWR Chemicals, Radnor, PA, USA, 40%). Microwave digestion was carried out in an Ethos UP reactor. After cooling down, the elemental analysis was carried out using an external calibration method (Ruthenium, AAS standard solution, Specpure, Ru 1000 µg/mL). All ICP analyses were carried out in duplo. The measurement error was evaluated based on calibration certificates and from statistical analysis of repeated measurements. The following errors were taken into account: the error of volumetric operations (pipettes, volumetric flasks, measuring cylinders), the error of balances and the error of concentrations/purity of commercial chemicals. For calculations,

calibration certificates or information sheets from the manufacturer were used. The main contributors were the error of calibration reference materials (1%) and the error of delivered volumes/masses. The absolute error did not exceed 1%.

### 3.3. Catalysis Experiments

For the photomethanation experiments, a custom-built photoreactor equipped with a solar simulator (Newport Sol3A, Newport Corporation, Irvine, CA, USA) and reaction cell with quartz window was used, as reported previously [33]. The mass of catalyst powder for one experiment was 200 mg. Every experiment was carried out according to the following procedure: the sample of catalyst powder on a quartz filter membrane was placed inside the reactor cell, after which the cap was closed tightly. Then, the temperature was stabilized at the desirable point with the internal heater. After temperature stabilization, the reactor was filled with the reaction mixture in the ratio  $\text{H}_2:\text{N}_2:\text{CO}_2$  (4.5:1:1). The total pressure before the experiment was  $3.5 \pm 0.2$  bars. During the experiments with non-zero light intensity, the sample was irradiated with a solar light simulator (provided with a filter of air mass coefficient 1.5 (AM 1.5)) from the top through the quartz window ( $1 \text{ sun} = 0.1 \text{ W}\cdot\text{cm}^{-2}$ ). Once the light source was switched on, gas samples (5 to 7 mL) were taken every 2.5 or 5 min from the upper part of the reactor using a gas-tight syringe and directly analyzed by gas chromatography (compact GC Interscience, Interscience, Breda, The Netherlands). GC is equipped with three channels, two micro TCD detectors and one FID detector. The first channel used to measure  $\text{H}_2$ ,  $\text{O}_2$ ,  $\text{N}_2$  and  $\text{CO}$  has a MolSieve 5 Å column and RT-Q bond precolumn and TCD detector. The second channel, used to measure  $\text{H}_2\text{O}$  and  $\text{CO}_2$ , has a combination of the TR-U bond column and RT-Q bond column and TCD detector. The third channel, used to measure methane, ethane and propane, is fitted with a Rtx-1, 2u column and FID detector. The standard deviation for every measurement was based on the error of balance, equipment (gas chromatography machine, pressure sensor, temperature sensor, light source), and measuring tools such as syringes. The absolute error did not exceed 2%. For calibration curves for the GC quantification and a representative gas chromatogram, see Figures S5 and S6.

## 4. Conclusions

We successfully prepared small spheroidal Ru nanoparticles on the surface of Stöber  $\text{SiO}_2$  and  $\gamma\text{-Al}_2\text{O}_3$  using two different preparation techniques: impregnation of the metal oxide with  $\text{Ru}_3(\text{CO})_{12}$  and subsequent thermal decomposition under  $\text{N}_2$  inert gas atmosphere, and deposition-precipitation followed by chemical reduction using  $\text{RuCl}_3$  as Ru precursor. Taking into account the difference in particle size of Ru obtained using both preparation techniques on  $\gamma\text{-Al}_2\text{O}_3$  (0.8–1.2 nm) and Stöber  $\text{SiO}_2$  (2.5–3.4 nm), the activity ( $0.14\text{--}0.63 \text{ mol}\cdot\text{g}_{\text{Ru}}^{-1}\cdot\text{h}^{-1}$ ) and selectivity ( $\geq 99\%$ ) of the catalysts for the sunlight-powered Sabatier process were similar. Ergo, the use of toxic and volatile  $\text{Ru}_3(\text{CO})_{12}$  can be avoided, since catalysts prepared by chemical reduction of  $\text{RuCl}_3$  display similar catalytic performance. However, the potential for reuse of Ru/ $\text{SiO}_2$  was better for catalysts obtained using  $\text{Ru}_3(\text{CO})_{12}$  as precursor. Catalysts prepared using  $\text{RuCl}_3$  suffered from progressive agglomeration of Ru nanoparticles on the  $\text{SiO}_2$  surface, resulting in a decrease in reaction rate of 28% between the first and the third run. Future work in our group will focus on improving the stability of Ru catalysts prepared by deposition-precipitation followed by chemical reduction using  $\text{RuCl}_3$  as Ru precursor to improve their potential for reuse.

**Supplementary Materials:** The following supporting information can be downloaded at: <https://www.mdpi.com/article/10.3390/catal12030284/s1>, Figure S1: X-ray diffractogram of  $\text{SiO}_2$  supported Ru catalyst prepared by reduction of  $\text{RuCl}_3$ , Figure S2: Thermogravimetric analyses of (a)  $\text{SiO}_2$ -supported and (b)  $\text{Al}_2\text{O}_3$ -supported Ru catalyst prepared by reduction of  $\text{RuCl}_3$ , under air, Figure S3: Conversion-time profile for three sequential runs of the sunlight-powered Sabatier reaction with Ru/ $\text{SiO}_2$ -TD, Figure S4: Comparison of mean diameter of Ru nanoparticles and numbers of agglomerates before (a) and after (b) reaction for Ru/ $\text{SiO}_2$ -CR catalysts with a Ru loading on silica of 3.34% w/w, Figure S5: Calibration curves for GC detection of (a)  $\text{H}_2$ , (b)  $\text{N}_2$ , (c)  $\text{CO}_2$  and (d)  $\text{CH}_4$ ,

Figure S6: Prototypical gas chromatogram for catalytic conversion of CO<sub>2</sub> and H<sub>2</sub> to CH<sub>4</sub> in a mixture diluted with N<sub>2</sub>.

**Author Contributions:** Conceptualization, M.K.V.B., P.B., A.H. and K.E.; methodology, D.B., J.R., F.S., P.B. and P.M.M.; validation, D.B., J.R. and P.M.M.; formal analysis, D.B. and P.B.; investigation, D.B., F.S. and P.M.M.; characterization, D.B., K.E., M.A.V. and A.-S.K.; writing—original draft preparation, D.B.; writing—review and editing, P.B., F.S., M.K.V.B., A.H., K.E. and N.M.; supervision, P.B., K.E., A.H. and M.K.V.B.; project administration, K.E. and N.M.; funding acquisition, P.B. and N.M. All authors have read and agreed to the published version of the manuscript.

**Funding:** This research was funded by the European Commission (H2020 project SPOTLIGHT, grant no. 722788).

**Acknowledgments:** M.A.V. acknowledges Solliance and the Dutch province of Noord-Brabant for funding the TEM facility. We acknowledge Ulrique Vounckx for performing TEM analyses.

**Conflicts of Interest:** The authors declare no conflict of interest.

## References

1. Sabatier, P.; Senderens, J.B. New Synthesis of Methane. In *Comptes Rendus Hebdomadaires des Seances de l'Academie des Sciences; Biodiversity Heritage Library*: Washington, DC, USA, 1902; Volume 134, pp. 514–516.
2. Martínez, J.; Hernández, E.; Alfaro, S.; Medina, R.L.; Aguilar, G.V.; Albitzer, E.; Valenzuela, M.A. High Selectivity and Stability of Nickel Catalysts for CO<sub>2</sub> Methanation: Support Effects. *Catalysts* **2019**, *9*, 24. [[CrossRef](#)]
3. Vogt, C.; Monai, M.; Kramer, G.J.; Weckhuysen, B.M. The renaissance of the Sabatier reaction and its applications on Earth and in space. *Nat. Catal.* **2019**, *2*, 188–197. [[CrossRef](#)]
4. Rönsch, S.; Schneider, J.; Matthischke, S.; Schlüter, M.; Götz, M.; Lefebvre, J.; Prabhakaran, P.; Bajohr, S. Review on methanation—From fundamentals to current projects. *Fuel* **2016**, *166*, 276–296. [[CrossRef](#)]
5. Sabatier, P.; Senderens, J.-B. Direct Hydrogenation of Oxides of Carbon in Presence of Various Finely Divided Metals. *CR Acad. Sci.* **1903**, *134*, 689–691.
6. Mendonça, C.D.; Khan, S.U.; Rahemi, V.; Verbruggen, S.W.; Machado, S.A.S.; De Wael, K. Surface plasmon resonance-induced visible light photocatalytic TiO<sub>2</sub> modified with AuNPs for the quantification of hydroquinone. *Electrochim. Acta* **2021**, *389*, 138734. [[CrossRef](#)]
7. Sarhan, R.M.; Koopman, W.; Pudell, J.; Stete, F.; Rössle, M.; Herzog, M.; Schmitt, C.N.Z.; Liebig, F.; Koetz, J.; Bargheer, M. Scaling Up Nanoplasmon Catalysis: The Role of Heat Dissipation. *J. Phys. Chem. C* **2019**, *123*, 9352–9357. [[CrossRef](#)]
8. Cortés, E.; Besteiro, L.V.; Alabastri, A.; Baldi, A.; Tagliabue, G.; Demetriadou, A.; Narang, P. Challenges in Plasmonic Catalysis. *ACS Nano* **2020**, *14*, 16202–16219. [[CrossRef](#)]
9. Murray, W.; Barnes, W. Plasmonic materials. *Adv. Mater.* **2007**, *19*, 3771–3782. [[CrossRef](#)]
10. Meng, X.; Wang, T.; Liu, L.; Ouyang, S.; Li, P.; Hu, H.; Kako, T.; Iwai, H.; Tanaka, A.; Ye, J. Photothermal Conversion of CO<sub>2</sub> into CH<sub>4</sub> with H<sub>2</sub> over Group VIII Nanocatalysts: An Alternative Approach for Solar Fuel Production. *Angew. Chem. Int. Ed.* **2014**, *53*, 11478–11482. [[CrossRef](#)]
11. Reddy, N.L.; Rao, V.N.; Vijayakumar, M.; Santhosh, R.; Anandan, S.; Karthik, M.; Shankar, M.V.; Reddy, K.R.; Shetti, N.P.; Nadagouda, M.N.; et al. A review on frontiers in plasmonic nano-photocatalysts for hydrogen production. *Int. J. Hydrogen Energy* **2019**, *44*, 10453–10472. [[CrossRef](#)]
12. Sanz, J.M.; Ortiz, D.; Alcaraz de la Osa, R.; Saiz, J.M.; González, F.; Brown, A.S.; Losurdo, M.; Everitt, H.O.; Moreno, F. UV Plasmonic Behavior of Various Metal Nanoparticles in the Near- and Far-Field Regimes: Geometry and Substrate Effects. *J. Phys. Chem. C* **2013**, *117*, 19606–19615. [[CrossRef](#)]
13. Lunde, P.J.; Kester, F.L. Carbon Dioxide Methanation on a Ruthenium Catalyst. *Ind. Eng. Chem. Process Des. Dev.* **1974**, *13*, 27–33. [[CrossRef](#)]
14. Sastre, F.; Versluis, C.; Meulendijks, N.; Rodríguez-Fernández, J.; Sweelssen, J.; Elen, K.; Van Bael, M.K.; den Hartog, T.; Verheijen, M.A.; Buskens, P. Sunlight-Fueled, Low-Temperature Ru-Catalyzed Conversion of CO<sub>2</sub> and H<sub>2</sub> to CH<sub>4</sub> with a High Photon-to-Methane Efficiency. *ACS Omega* **2019**, *4*, 7369–7377. [[CrossRef](#)]
15. Aziz, M.A.A.; Jalil, A.A.; Triwahyono, S.; Ahmad, A. CO<sub>2</sub> methanation over heterogeneous catalysts: Recent progress and future prospects. *Green Chem.* **2015**, *17*, 2647–2663. [[CrossRef](#)]
16. Veith, G.M.; Lupini, A.R.; Rashkeev, S.; Pennycook, S.J.; Mullins, D.R.; Schwartz, V.; Bridges, C.A.; Dudney, N.J. Thermal stability and catalytic activity of gold nanoparticles supported on silica. *J. Catal.* **2009**, *262*, 92–101. [[CrossRef](#)]
17. Martin, N.M.; Hemmingsson, F.; Wang, X.; Merte, L.R.; Hejral, U.; Gustafson, J.; Skoglundh, M.; Meira, D.M.; Dippel, A.; Gutowski, O.; et al. Structure-function Relationship during CO<sub>2</sub> Methanation over Rh/Al<sub>2</sub>O<sub>3</sub> and Rh/SiO<sub>2</sub> Catalysts at Atmospheric Pressure Conditions. *Catal. Sci. Technol.* **2018**, *8*, 2686–2696. [[CrossRef](#)]
18. Chai, S.; Men, Y.; Wang, J.; Liu, S.; Song, Q.; An, W.; Kolb, G. Boosting CO<sub>2</sub> methanation activity on Ru/TiO<sub>2</sub> catalysts by exposing (001) facets of anatase TiO<sub>2</sub>. *J. CO<sub>2</sub> Util.* **2019**, *33*, 242–252. [[CrossRef](#)]

19. Lin, Q.; Liu, X.Y.; Jiang, Y.; Wang, Y.; Huang, Y.; Zhang, T. Crystal phase effects on the structure and performance of ruthenium nanoparticles for CO<sub>2</sub> hydrogenation. *Catal. Sci. Technol.* **2014**, *4*, 2058–2063. [[CrossRef](#)]
20. Garbarino, G.; Bellotti, D.; Finocchio, E.; Magistri, L.; Busca, G. Methanation of carbon dioxide on Ru/Al<sub>2</sub>O<sub>3</sub>: Catalytic activity and infrared study. *Catal. Today* **2016**, *277*, 21–28. [[CrossRef](#)]
21. Tada, S.; Shimizu, T.; Kameyama, H.; Haneda, T.; Kikuchi, R. Ni/CeO<sub>2</sub> catalysts with high CO<sub>2</sub> methanation activity and high CH<sub>4</sub> selectivity at low temperatures. *Int. J. Hydrogen Energy* **2012**, *37*, 5527–5531. [[CrossRef](#)]
22. Ashok, J.; Ang, M.L.; Kawi, S. Enhanced activity of CO<sub>2</sub> methanation over Ni/CeO<sub>2</sub>-ZrO<sub>2</sub> catalysts: Influence of preparation methods. *Catal. Today* **2017**, *281*, 304–311. [[CrossRef](#)]
23. Parapat, R.Y.; Saputra, O.H.I.; Ang, A.P.; Schwarze, M.; Schomacker, R. Hot Electron and Surface Plasmon-Driven Catalytic Reaction in Metal–Semiconductor Nanostructures. *RSC Adv.* **2014**, *4*, 50955. [[CrossRef](#)]
24. Murena, F.; Esposito, S.; Deorsola, F.A.; Galletti, C.; Prati, M.V. CO<sub>2</sub> abatement and CH<sub>4</sub> recovery at vehicle exhausts: Comparison and characterization of Ru powder and pellet catalysts. *Int. J. Hydrogen Energy* **2020**, *45*, 8640–8648. [[CrossRef](#)]
25. Porta, A.; Falbo, L.; Visconti, C.G.; Lietti, L.; Bassano, C.; Deiana, P. Synthesis of Ru-based catalysts for CO<sub>2</sub> methanation and experimental assessment of intraporous transport limitations. *Catal. Today* **2020**, *343*, 38–47. [[CrossRef](#)]
26. Zhang, X.; Li, X.; Reish, M.E.; Zhang, D.; Su, N.Q.; Gutiérrez, Y.; Moreno, F.; Yang, W.; Everitt, H.O.; Liu, J. Plasmon-Enhanced Catalysis: Distinguishing Thermal and Nonthermal Effects. *Nano Lett.* **2018**, *18*, 1714–1723. [[CrossRef](#)] [[PubMed](#)]
27. Karelovic, A.; Ruiz, P. CO<sub>2</sub> hydrogenation at low temperature over Rh/-Al<sub>2</sub>O<sub>3</sub> catalysts: Effect of the metal particle size on catalytic performances and reaction mechanism. *Appl. Catal. B Environ.* **2012**, *113–114*, 237–249. [[CrossRef](#)]
28. Avanesian, T.; Gusmão, G.S.; Christopher, P. Mechanism of CO<sub>2</sub> reduction by H<sub>2</sub> on Ru(0 0 1) and general selectivity descriptors for late-transition metal catalysts. *J. Catal.* **2016**, *343*, 86–96. [[CrossRef](#)]
29. Wang, F.; He, S.; Chen, H.; Wang, B.; Zheng, L.; Wei, M.; Evans, D.G.; Duan, X. Active Site Dependent Reaction Mechanism over Ru/CeO<sub>2</sub> Catalyst toward CO<sub>2</sub> Methanation. *J. Am. Chem. Soc.* **2016**, *138*, 6298–6305. [[CrossRef](#)]
30. Kim, C.; Hyeon, S.; Lee, J. Energy-efficient CO<sub>2</sub> hydrogenation with fast response using photoexcitation of CO<sub>2</sub> adsorbed on metal catalysts. *Nat. Commun.* **2018**, *9*, 3027. [[CrossRef](#)]
31. Kowalczyka, Z.; Stołecik, K.; Rarog-Pilecka, W.; Miskiewicz, E.; Wilczkowska, E.; Karpinski, Z. Supported ruthenium catalysts for selective methanation of carbon oxides at very low CO<sub>x</sub>/H<sub>2</sub> ratios. *Appl. Catal. A Gen.* **2008**, *342*, 35–39. [[CrossRef](#)]
32. Van der Zwaan, B.; Detz, R.; Meulendijks, N.; Buskens, P. Renewable natural gas as climate-neutral energy carrier? *Fuel* **2022**, *311*, 122547. [[CrossRef](#)]
33. Grote, R.; Habets, R.; Rohlfs, J.; Sastre, F.; Meulendijks, N.; Xu, M.; Verheijen, M.A.; Elen, K.; Hardy, A.; Van Bael, M.K.; et al. Collective photothermal effect of Al<sub>2</sub>O<sub>3</sub>-supported spheroidal plasmonic Ru nanoparticle catalysts in the sunlight-powered Sabatier reaction. *ChemCatChem* **2020**, *12*, 5618–5622. [[CrossRef](#)]
34. Rohlfs, J.; Bossers, K.W.; Meulendijks, N.; Valega Mackenzie, F.; Xu, M.; Verheijen, M.A.; Buskens, P.; Sastre, F. Continuous-Flow Sunlight-Powered CO<sub>2</sub> Methanation Catalyzed by γ-Al<sub>2</sub>O<sub>3</sub>-Supported Plasmonic Ru Nanorods. *Catalysts* **2022**, *12*, 126. [[CrossRef](#)]
35. Xu, M.; den Hartog, T.; Cheng, L.; Wolfs, M.; Habets, R.; Rohlfs, J.; van den Ham, J.; Meulendijks, N.; Sastre, F.; Buskens, P. Using Fiber Bragg Grating Sensors to Quantify Temperature Non-Uniformities in Plasmonic Catalyst Beds under Illumination. *ChemPhotoChem* **2022**. accepted for publication. [[CrossRef](#)]
36. Sharma, S.; Hu, Z.; Zhang, P.; McFarland, E.W.; Metiu, H. CO<sub>2</sub> methanation on Ru-doped ceria. *J. Catal.* **2011**, *278*, 297–309. [[CrossRef](#)]
37. Lach, D.; Zhdan, U.; Smolinski, A.; Polanski, J. Functional and material properties in nanocatalyst design: A data handling and sharing problem. *Int. J. Mol. Sci.* **2021**, *22*, 5176. [[CrossRef](#)]
38. Stöber, W.; Fink, A.; Bohn, E. Controlled Growth of Monodisperse Silica Spheres in the Micron Size Range. *J. Colloid Interface Sci.* **1968**, *26*, 62–69. [[CrossRef](#)]